Electronic Supplementary Material (ESI) for New Journal of Chemistry.

Supporting Information

Luminescent Coordination Polymers Based on Ca^{2+} and Octahedral Cluster Anions $[\{M_6Cl^i_8\}Cl^a_6]^{2-}$ (M = Mo, W): Synthesis and Thermal Stability Studies

Darya V. Evtushok,[a,b] Natalya A. Vorotnikova,[a,b] Vladimir A. Logvinenko,[a,c] Anton I. Smolentsev,[a,c] Konstantin A. Brylev,[a,b,c] Pavel E. Plyusnin,[a,c] Denis P. Pishchur,[a] Noboru Kitamura,[d] Yuri V. Mironov,[a,b,c] Anastasiya O. Solovieva,[b] Olga A. Efremova[e*] and Michael A. Shestopalov[a,b,c*]

[a]*Nikolaev Institute of Inorganic Chemistry SB RAS, 3 Acad. Lavrentiev Prospect, 630090 Novosibirsk, Russia, E-mail: shtopy@niic.nsc.ru; Tel: +73833309253.*

[b]*Research Institute of Clinical and Experimental Lymphology – Branch of the ICG SB RAS, 2 Timakova Str., 630060 Novosibirsk, Russia.*

[c]*Novosibirsk State University, 2 Pirogova st., 630090 Novosibirsk, Russia.*

[d]*Department of Chemistry, Faculty of Science, Hokkaido University, 060-0810 Sapporo, Japan.*

[e]*School of Mathematics and Physical Sciences, University of Hull, Cottingham Road, HU6 7RX, Hull, UK. E-mail: o.efremova@hull.ac.uk; Tel: +44 (0)1482 465417*

Content

Crystallographic data and selected interatomic distances for compounds 1, 2 and 4 3
FTIR-spectra of 1-4 5
The solid-phase transformation 6
X-ray powder diffraction patterns 7
Thermal and kinetic analysis 8
Defuse reflectance spectra 15

Crystallographic data and selected interatomic distances for compounds 1, 2 and 4

Table S1. Crystallographic data, data collection and structure refinement details for **1**, **2** and **4**.

	1	**2**	**4**
Empirical formula	$C_{76}H_{70}CaCl_{14}Mo_6N_2O_6P_4$	$C_{76}H_{70}CaCl_{14}N_2O_6P_4W_6$	$C_{72}H_{60}CaCl_{14}O_4P_4W_6$
Formula weight	2343.24	2870.70	2752.56
Crystal system	Monoclinic	Monoclinic	Monoclinic
Space group	*C*2/*c*	*C*2/*c*	*C*2/*c*
a, Å	23.021(5)	22.955(5)	25.3726(10)
b, Å	16.305(3)	16.219(3)	14.1362(6)
c, Å	24.931(5)	24.818(5)	24.2685(11)
β, º	108.69(3)	108.58(3)	113.2120(10)
V, Å^3	8864(3)	8758(3)	7999.8(6)
Z	4	4	4
ρ_{calc}, g cm^{-3}	1.756	2.174	2.285
μ, mm^{-1}	1.425	8.457	9.251
Crystal size, mm^3	0.28 × 0.26 × 0.17	0.50 × 0.50 × 0.40	0.20 × 0.20 × 0.15
θ range, º	1.56–32.52	3.05–27.48	1.83–27.51
h, *k*, *l* ranges	$-34 \le h \le 34$ $-24 \le k \le 24$ $-37 \le l \le 18$	$-23 \le h \le 29$ $-20 \le k \le 20$ $-29 \le l \le 32$	$-32 \le h \le 32$ $-18 \le k \le 18$ $-31 \le l \le 31$
Reflections collected	40747	30487	26998
Independent reflections (R_{int})	15414 (0.0263)	9576 (0.0740)	9037 (0.0496)
Observed reflections [$I > 2\sigma(I)$]	10680	6739	6061
Parameters refined	499	499	458
$R_1[F^2 > 2\sigma(F^2)]$	0.0331	0.0616	0.0367
$wR_2(F^2)$	0.0829	0.1471	0.0818
GOOF on F^2	1.023	0.985	0.980
$\Delta\rho_{max}$, $\Delta\rho_{min}$, *e*Å^{-3}	0.755, –0.450	4.578, –3.327	1.522, –2.081

Table S2. Selected interatomic distances (Å) for **1** – **4**.

Bond length	**1**	**2**	**3**[a]	**4**
M–M	2.6018(9)–2.6125(6)	2.6170(8)–2.6240(7)	2.5919(4)–2.6043(4)	2.5984(4)–2.6173(4)
M–Cl[i]	2.4684(8)–2.4818(8)	2.490(3)–2.517(2)	2.453(1)–2.479(1)	2.487(2)–2.516(2)
M–Cl[a]	2.425(1)–2.4542(7)	2.425(3)–2.448(3)	2.402(1)–2.464(1)	2.403(2)–2.452(2)
Ca–Cl[a]	—	—	2.794(2)–2,831(2)	2.776(3)–2.783(3)
Ca–O_{H2O}	2.409(2)	2.378(8)	—	—
Ca–O_{OPPh3}	2.260(2)–2.337(2)	2.273(7)–2.335(6)	2.252(2)–2.257(2)	2.266(4)–2.275(4)

[a] Z. S. Kozhomuratova, Y. V. Mironov, M. A. Shestopalov, Y. M. Gaifulin, N. V. Kurat'eva, E. M. Uskov and V. E. Fedorov, *Russ. J. Coord. Chem.*, 2007, **33**, 1-6.

FTIR-spectra of 1-4

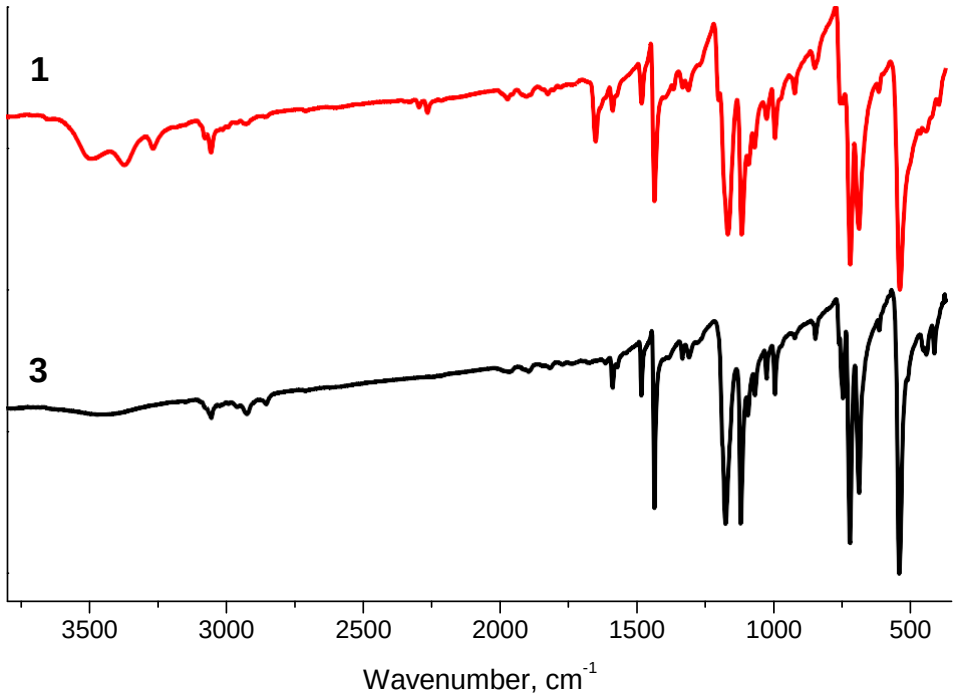

Figure S1. FTIR-spectra of [*cis*-$Ca(OPPh_3)_4(H_2O)_2$][{$Mo_6Cl^i_8$}Cl^a_6]·$2CH_3CN$ (**1**), *trans*-[{$Ca(OPPh_3)_4$}{{$Mo_6Cl^i_8$}Cl^a_6}]$_\infty$ (**3**).

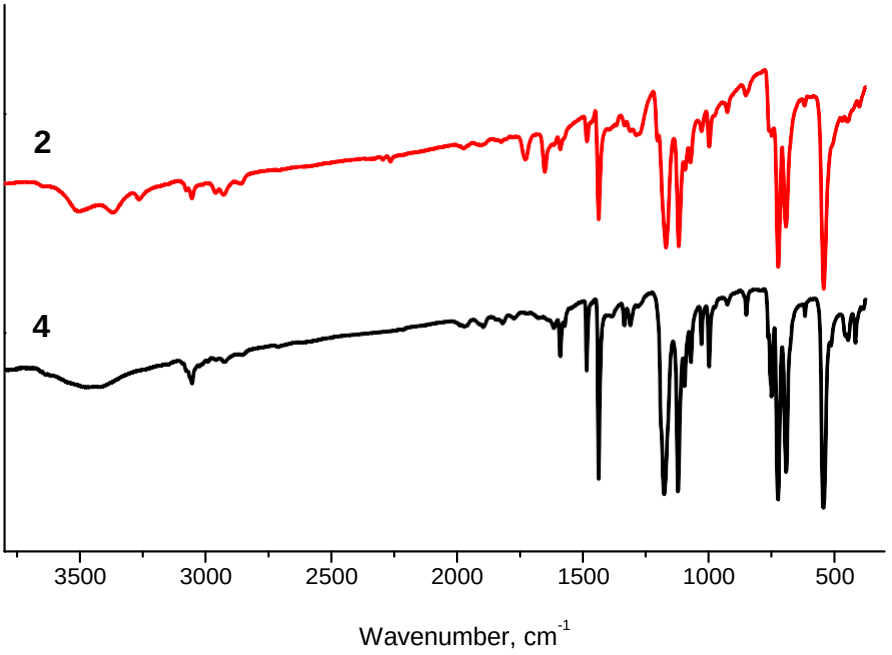

Figure S2. FTIR-spectra of [*cis*-$Ca(OPPh_3)_4(H_2O)_2$][{$W_6Cl^i_8$}Cl^a_6]·$2CH_3CN$ (**2**), *trans*-[{$Ca(OPPh_3)_4$}{{$W_6Cl^i_8$}Cl^a_6}]$_\infty$ (**4**).

The solid-phase transformation

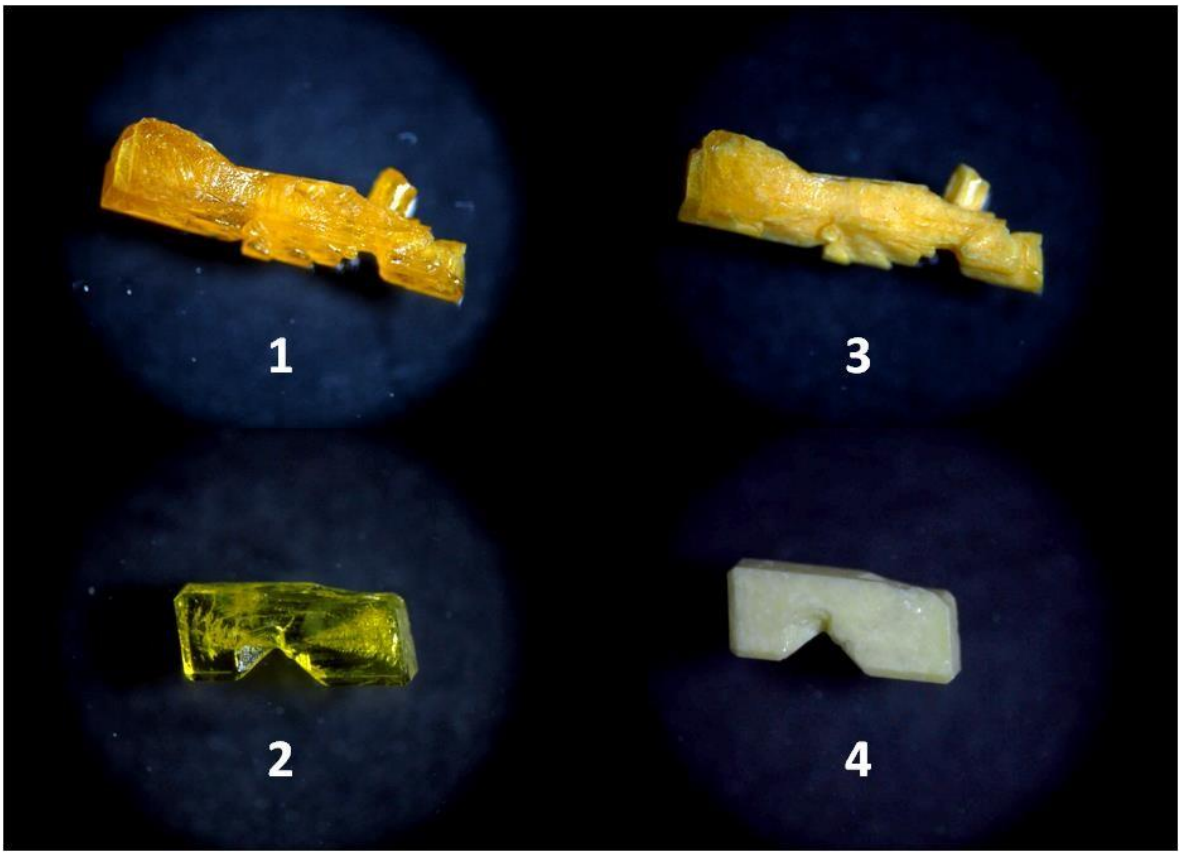

Figure S3. Crystals of **1** and **2** before and after heating at 110 °C for 10 min (i.e. after phase transition to **3** and **4**).

X-ray powder diffraction patterns

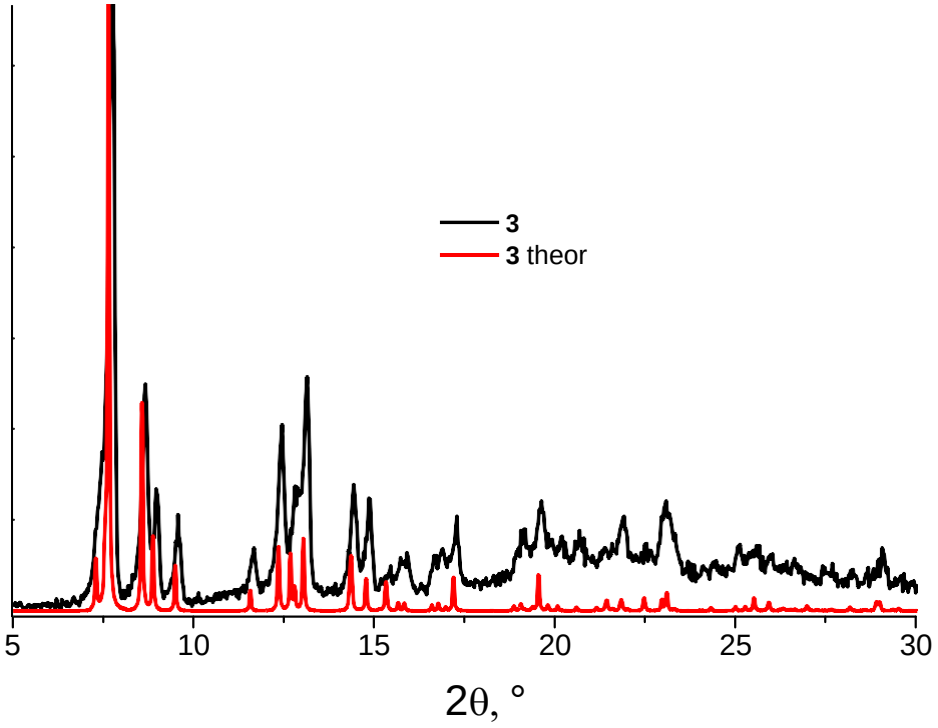

Figure S4. Experimental and simulated X-ray powder diffraction and theoretical diffraction patterns of *trans*-[{Ca(OPPh$_3$)$_4$}{{Mo$_6$Cl$^i_8$}Cl$^a_6$}]$_\infty$ (**3**).

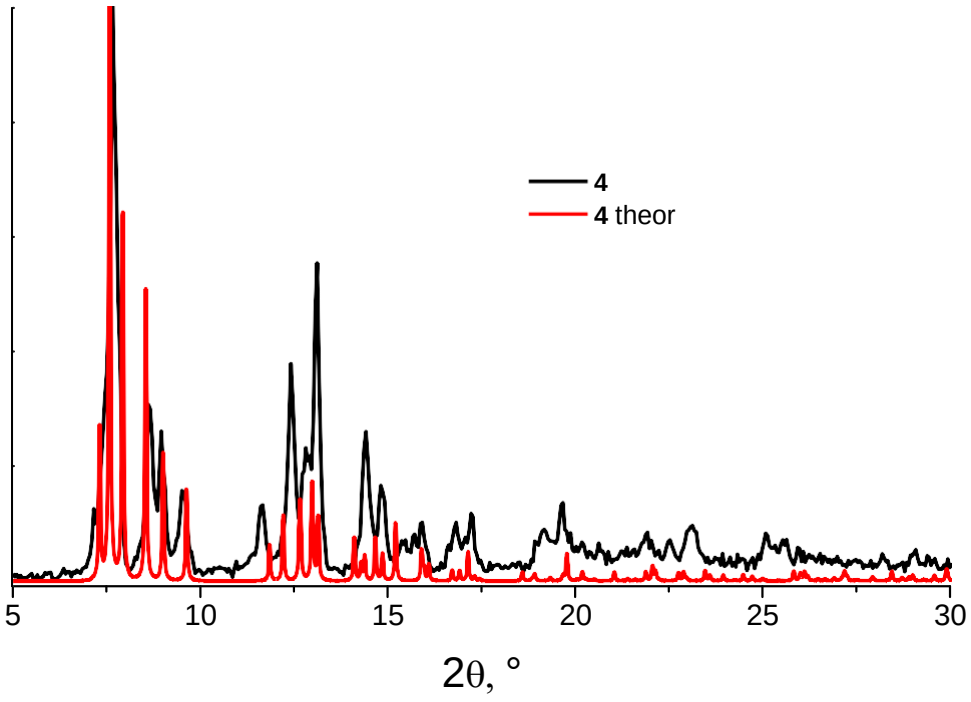

Figure S5. Experimental X-ray powder diffraction and theoretical diffraction patterns of *trans*-[{Ca(OPPh$_3$)$_4$}{{W$_6$Cl$^i_8$}Cl$^a_6$}]$_\infty$ (**4**).

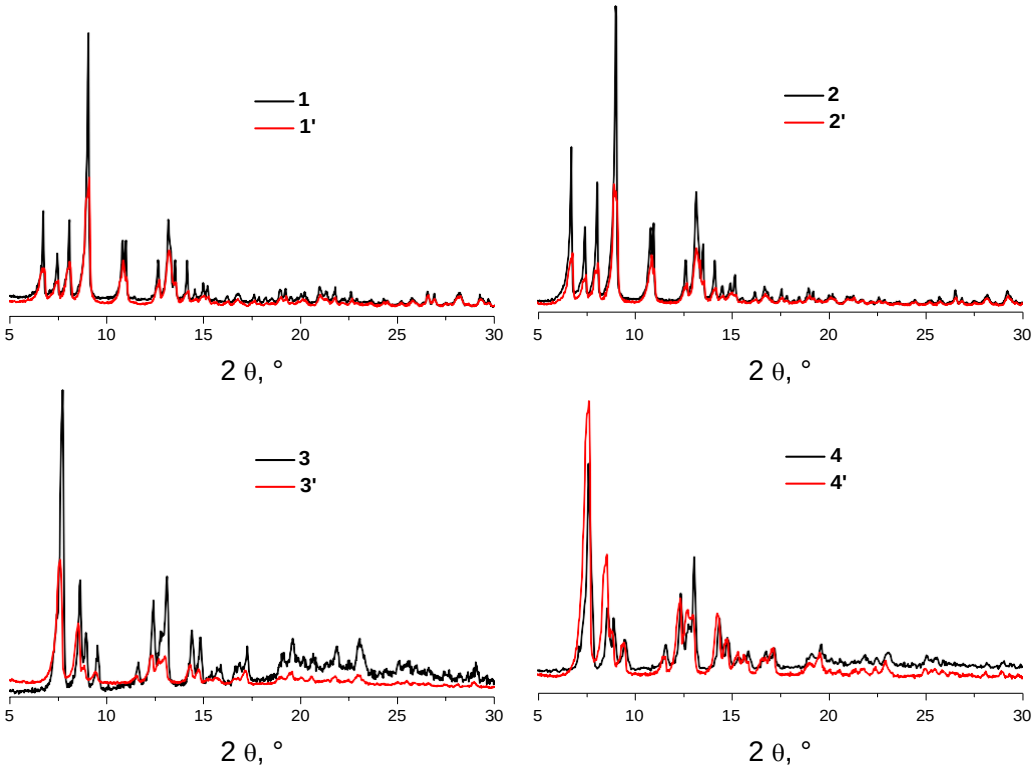

Figure S6. X-ray powder diffraction of compounds **1-4** fresh and after 1 week at ambient conditions (**1**'-**4**').

Thermal and kinetic analysis

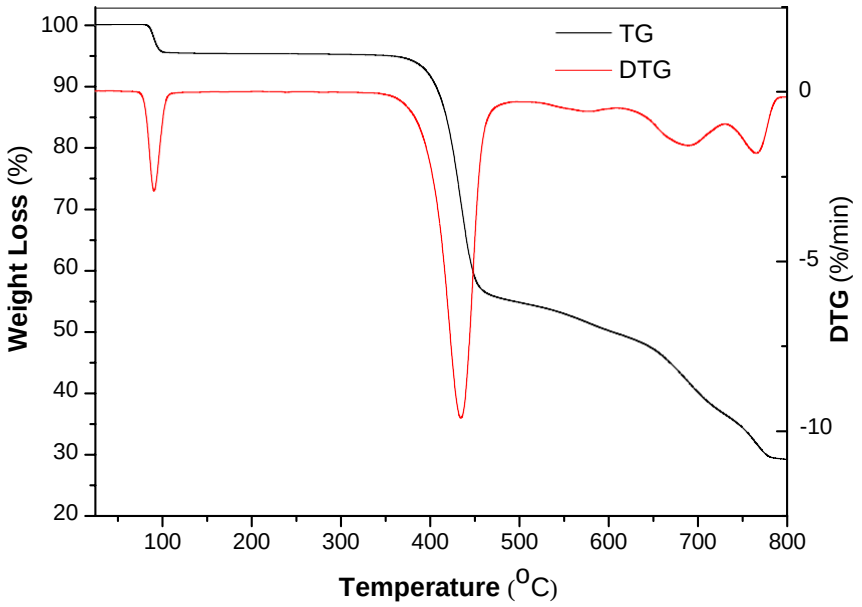

Figure S7. TGA/DTG curves of [*cis*-$Ca(OPPh_3)_4(H_2O)_2$][{$Mo_6Cl^i_8$}Cl^a_6]·$2CH_3CN$ (**1**).

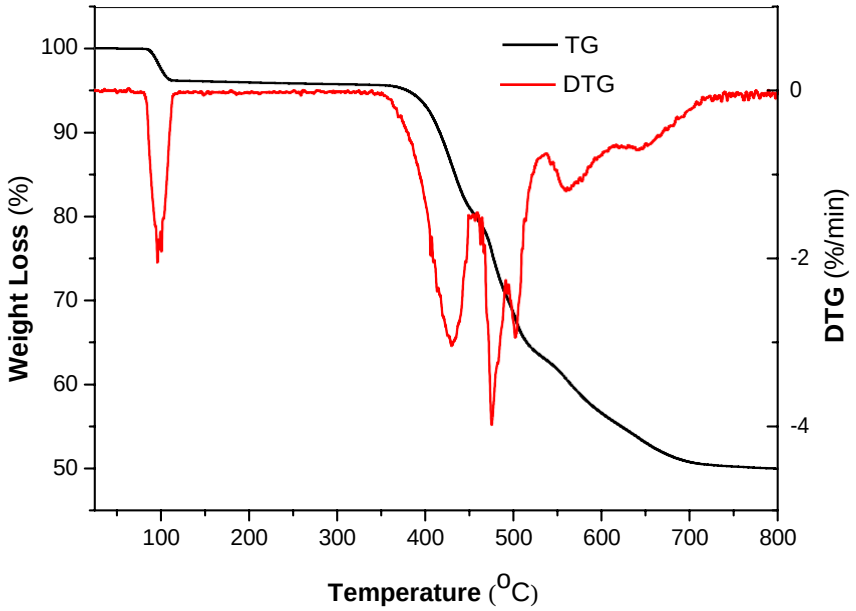

Figure S8. TGA/DTG curves of [*cis*-Ca(OPPh$_3$)$_4$(H$_2$O)$_2$][{W$_6$Cl$^i_8$}Cl$^a_6$]·2CH$_3$CN (**2**).

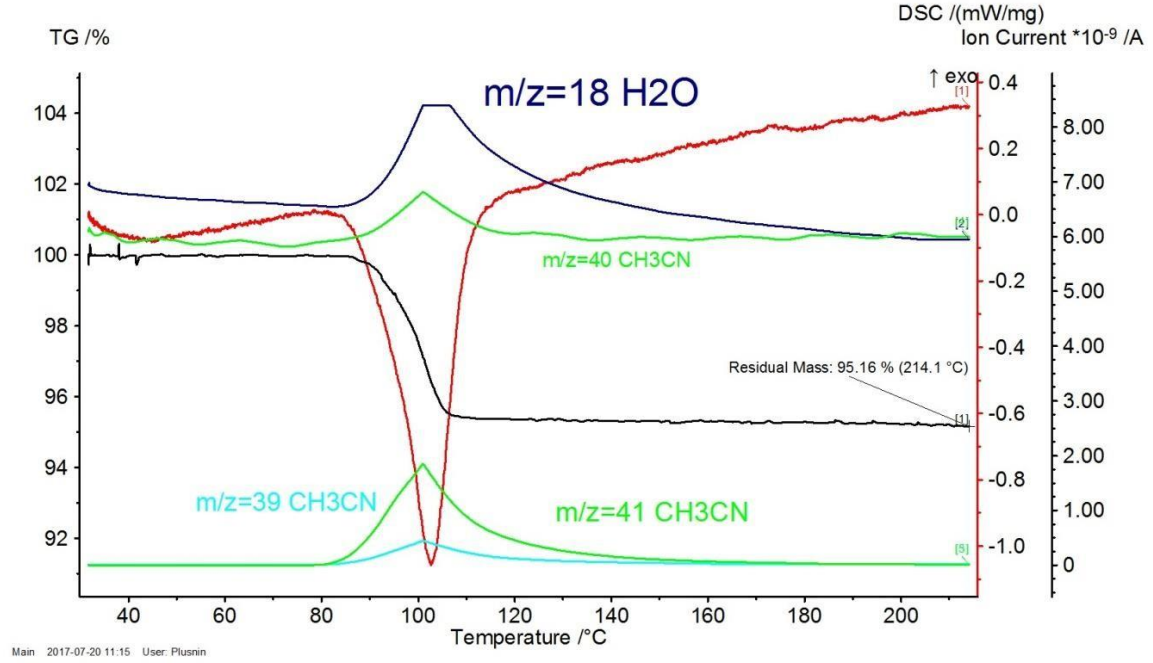

Figure S9. The thermal decomposition of **1** studied by STA at heating rate 20 K min^{-1}: black is the TG curve; red is the DSC curve; green and cyan are the curves of acetonitrile gas evolution, navy blue is the curve of water evolution.

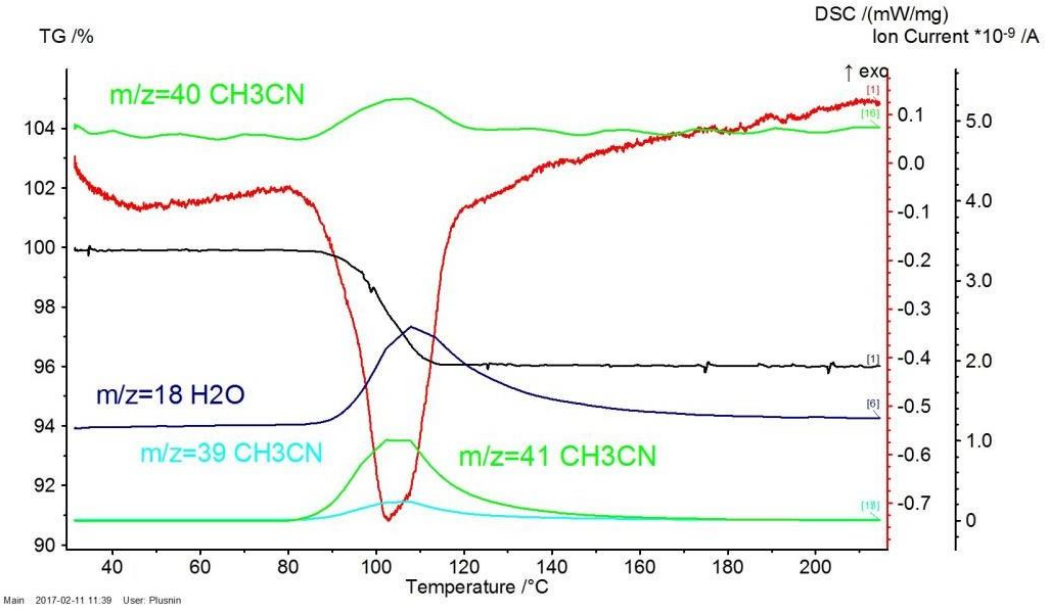

Figure S10. The thermal decomposition of **2** studied by STA at heating rate 20 K min^{-1}: black is the TG curve; red is the DSC curve; green and cyan are the curves of acetonitrile gas evolution, navy blue is the curve of water evolution.

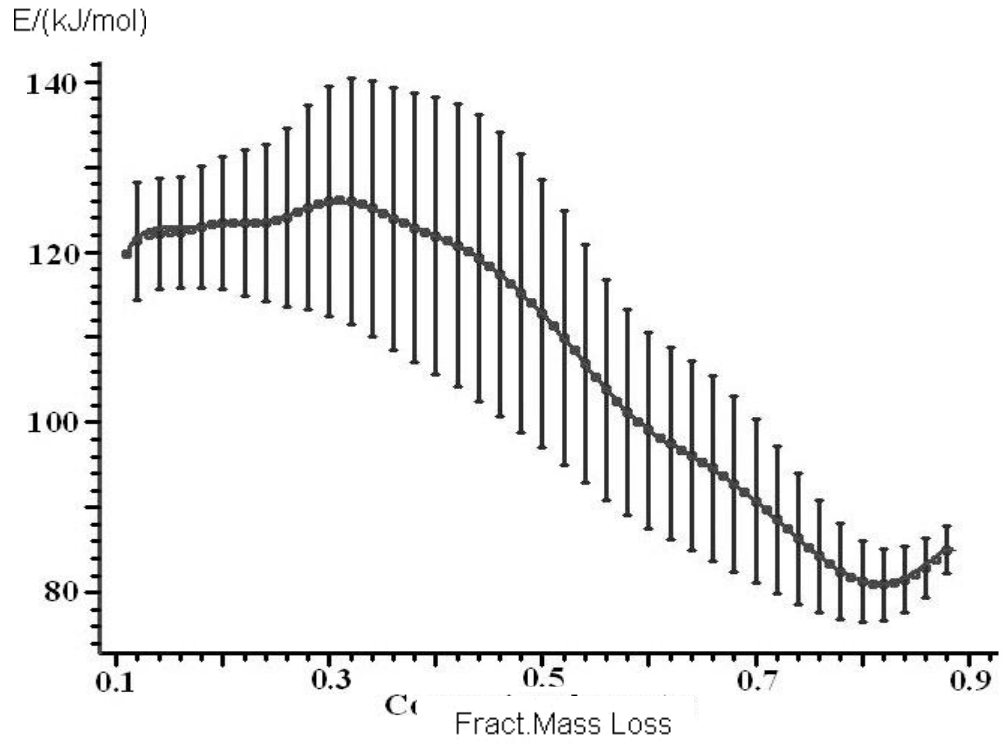

Figure S11. Friedman analysis of **1** thermal decomposition: activation energies depending on the degree of conversion α.

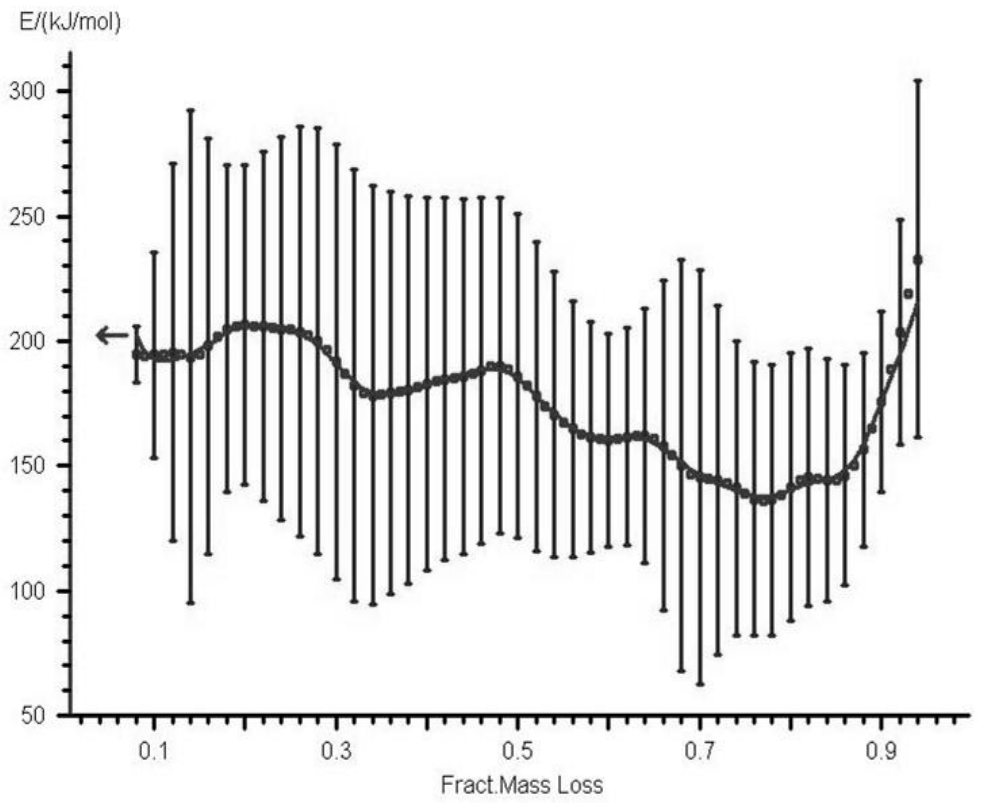

Figure S12. Friedman analysis of **2** thermal decomposition: activation energies depending on the degree of conversion α.

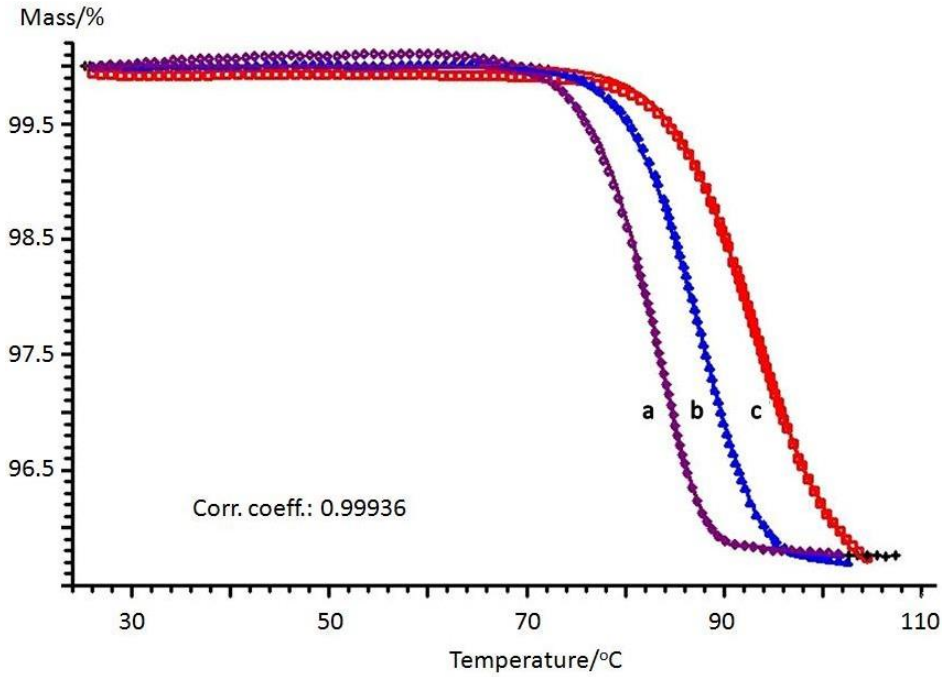

Figure S13. Data processing for **1** thermal decomposition. TG curve fitting of nonlinear regression, simulated with two consecutive reactions (the first one is An, the second one is Fn). The points are the experimental data; the lines are the calculated data. The heating rates were 5 (a), 10 (b), 20 (c) °C min^{-1}.

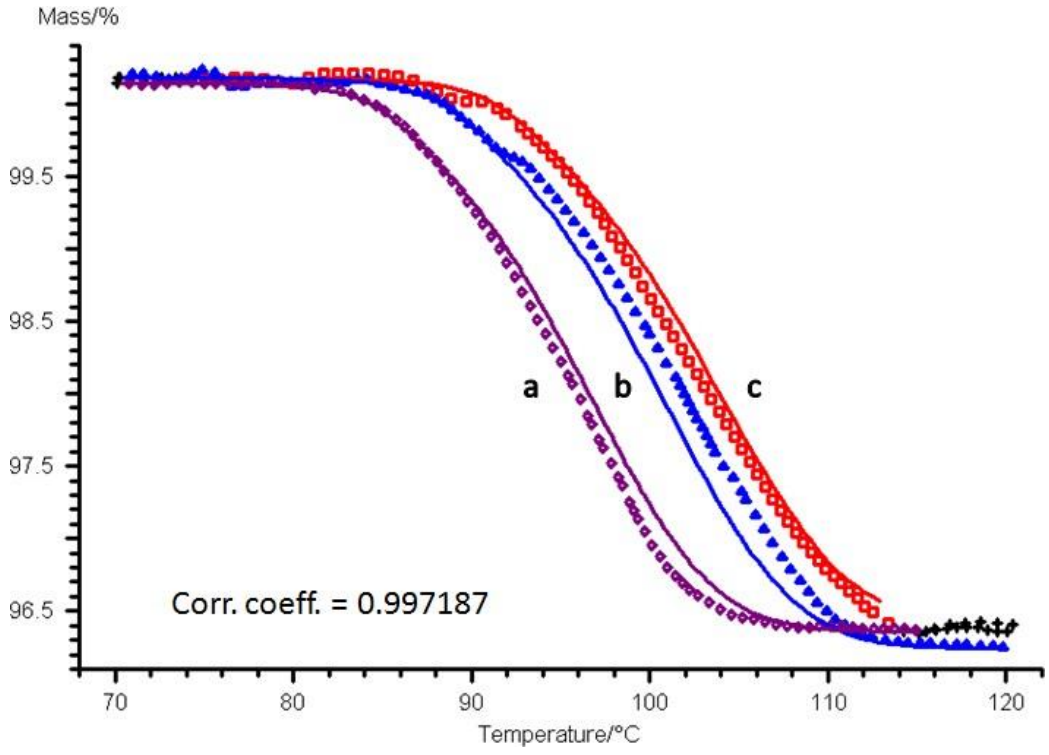

Figure S14. Data processing for **2** thermal decomposition. TG curve fitting of nonlinear regression, simulated with two consecutive reactions (both equations are An). The points are the experimental data; the lines are the calculated data. The heating rates were 5 (a), 10 (b), 20 (c) °C min^{-1}.

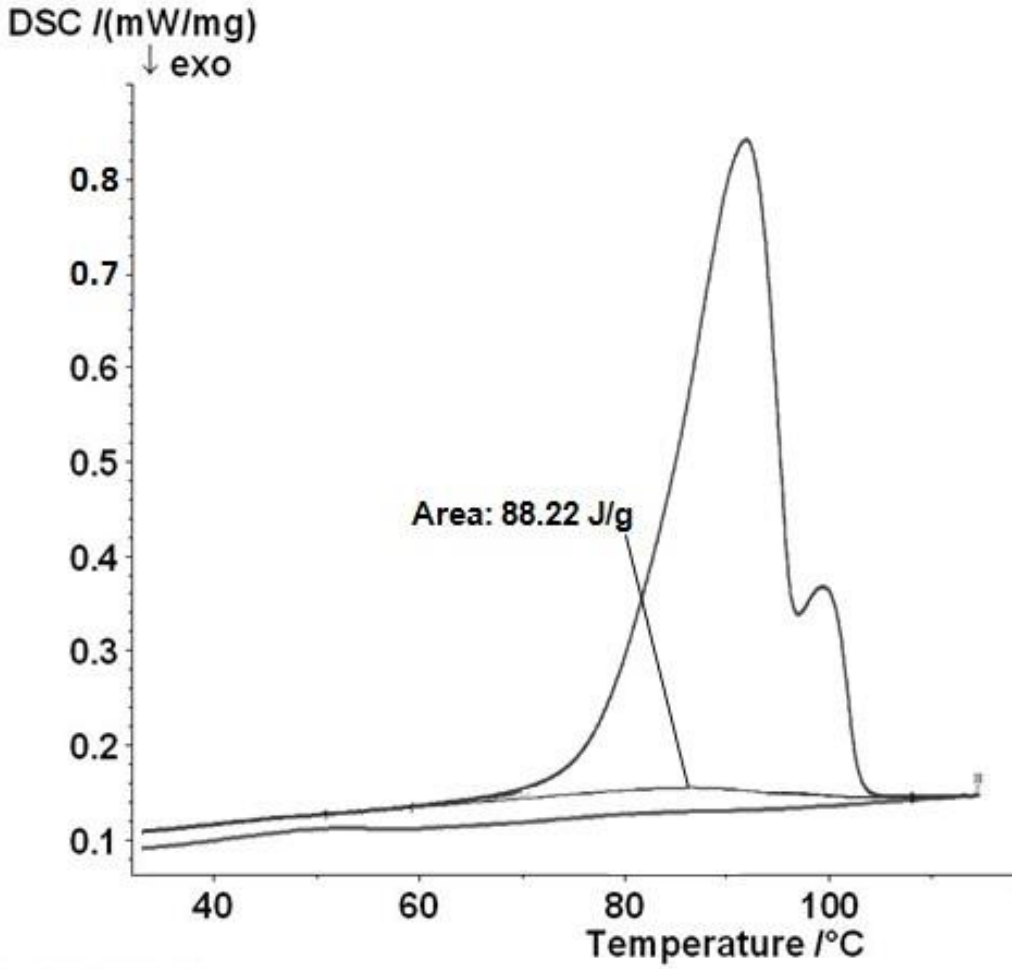

Figure S15. DSC analysis of **1**.

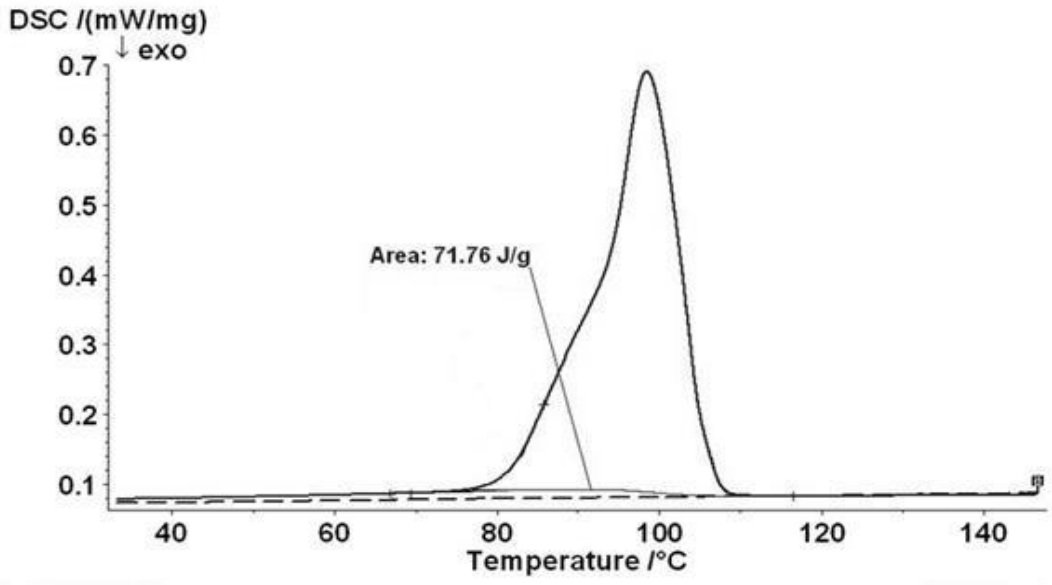

Figure S16. DSC analysis of **2**.

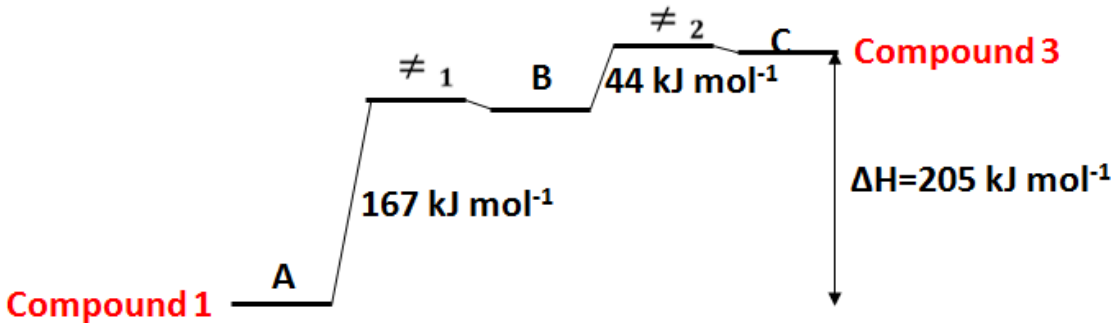

Scheme S1. The schematic representation of energy diagram for conversion of compound **1** to compound **3**.

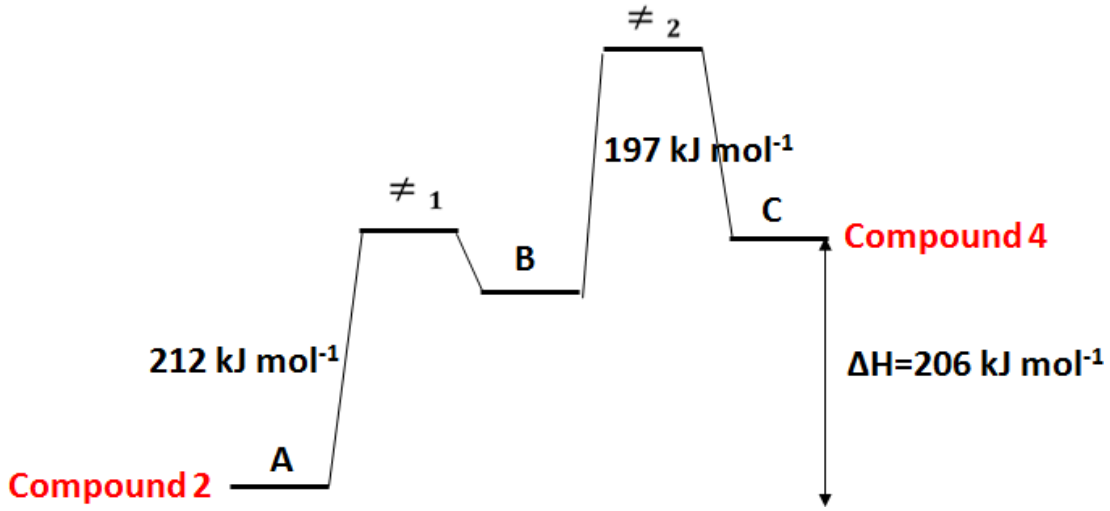

Scheme S2. The schematic representation of energy diagram for conversion of compound **2** to compound **4**.

Defuse reflectance spectra

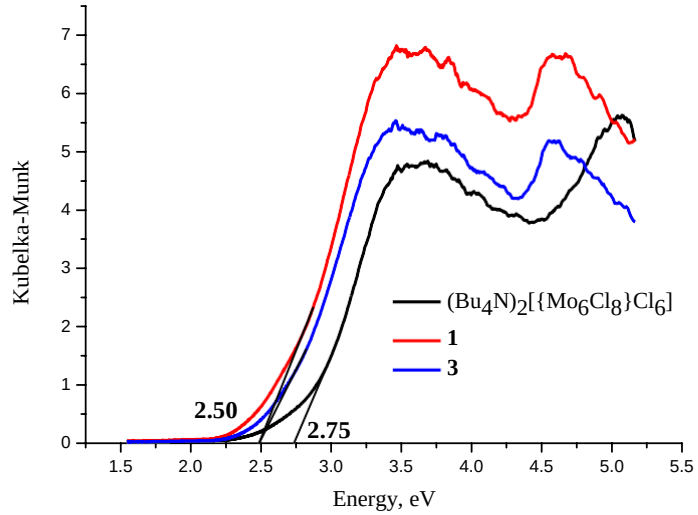

Figure S17. The defuse reflectance spectra of $(Bu_4N)_2[\{Mo_6Cl_8\}Cl_6]$, **1** and **3** represented in Kubelka-Munk units. The corresponding values of the optical band gaps obtained from Kubelka-Munk theory are shown in bold.

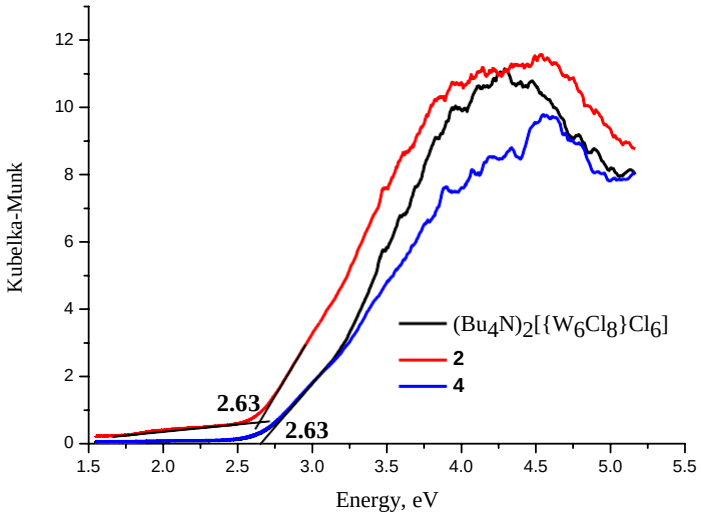

Figure S18. The defuse reflectance spectra of $(Bu_4N)_2[\{W_6Cl_8\}Cl_6]$, **2** and **4** represented in Kubelka-Munk units. The corresponding values of the optical band gaps obtained from Kubelka-Munk theory are shown in bold.